J. Basic. Appl. Sci. Res., 2(11)11774-11782, 2012
© 2012, TextRoad Publication

ISSN 2090-4304
Journal of Basic and Applied Scientific Research
www.textroad.com

Numerical Study on Sensitivity of PEM Fuel Cell's Output Power to Saturation at Non Isothermal Condition

Davoud Mostafa Tobnaghi[1], Ali Mirizadeh[2], Mehdi imanzadeh[3]

[1]Department of Electrical Engineering, Parsabad Moghan Branch, Islamic Azad University, Parsabad Moghan, Iran
[2]Department of Mechanical Engineering, Parsabad Moghan Branch, Islamic Azad University, Parsabad Moghan, Iran
[3]Department of chemistry, Parsabad Moghan Branch, Islamic Azad University, Parsabad Moghan, Iran

ABSTRACT

This study focus on two-dimensional, non-isothermal, two phases and steady state model to explore the effects of temperature gradient on liquid water accumulation in porous electrode of cathode at proton exchange membrane fuel cell and consequently its effect on output power. For this goal, a homemade FORTRAN code is developed to simulate transport phenomena in PEM fuel cell. Strongly coupled transport equation is discretized using power law scheme and solved by Stone's method. A comparison between isothermal and non- isothermal fuel cell models are made. Results reveal that the maximum liquid saturation is higher for the isothermal model than non-isothermal model and thermal gradient distribution in cell affects the saturation amount and its location at cathode section and cause saturation level decrease and shift to channel downstream. Therefore porous medium paths that blocked by saturation, opens for oxygen diffusion through gas diffusion layer and voltage lost due to mass diffusion problem decrease and hence PEM fuel cell output power increase .this study reveals that non-isothermal model give precise and real information of PEM fuel cell's transport phenomena. The results are in good agreement with available experimental data.
KEYWORDS: PEM fuel cell, temperature gradient, saturation, polarization curve, output power.

1. INTRODUCTION

PEM fuel cells are expected to be future's power generation device, there are still some technological limitations that are restricting these energy converter devices from becoming a commercial success. Performance of Fuel cell is evaluated by the relation between the cell potential and current density [1]. During fuel cell operation, water is produced in the cathode catalyst layer in the form of liquid, resulting in gas–liquid flow in the porous media and the channels [2, 3]. On the other hand, due to the low operating temperature of PEM fuel cells (30–100 ◦C), it may be the partial pressure of water vapor exceeds to the value of saturation pressure, condensation occurs [1, 4, 5]. If formed Liquid excessive water is not removed from the cathode, it may cause flooding of the cell resulting in a lower air flow rate on the cathode side, increasing the voltage loss due to mass transport limitation, leading to cell degradation [1].Therefore, water management, has been a critical challenge for a high-performance fuel cell design and optimization. A number of different computational approaches for PEM fuel cells have been carried out in recent years considering two-phase or single-phase water transport with or without heat transfer at proton exchange membrane regions [2-10]. Several studies [9, 11, 12] have attempted to predict the temperature distribution for single-phase condition. Two-phase transport in PEM fuel cells has also been studied by several researchers [13, 14]. However, the focus of these studies was primarily on the isothermal investigation of the transport phenomena. The two-phase non-isothermal model, gives a proper simultaneous description of water and thermal management with phase change. The model presented by [15, 5] illustrates the behaviors of the two-phase flow and heat transfer in a porous electrode. Wang et al. [16] first studied two-phase flow and liquid water transport on the cathode side of a PEM fuel cell based on the multiphase mixture model (M2 model) originally developed by Wang and Cheng.

The above literature review obviously indicates that water and thermal management are critical issues in investigations of PEM fuel cells. However, discussions concerning the effect of the saturation location on the cell performance and transport process are rarely seen. Therefore, in the present study, a two-dimensional, two-phase, non-isothermal, and steady state model together with coupled electrochemical relations is developed and the effects of temperature gradient distribution on water saturation are investigated. The model couples the flows, energy, species, electrical potential, and current density distributions in the cathode and anode fluid channels, gas diffusers, catalyst layers and membrane.

2. MATHEMATICAL MODELIG

The model domain comprises of the following sub regions: the gas channels, gas diffusion layers (GDLs), catalyst layers, with the membrane in the middle. Fuel and oxidant flow through channels and are distributed into anode

Corresponding Author: Ali Mirizadeh, Department of Mechanical Engineering, Parsabad Moghan Branch, Islamic Azad University, Parsabad Moghan, Iran.E-mail: ali.mirizadeh@gmail.com

and cathode, Fig.1.The fuel and oxidant flow rates can be described by a stoichiometric flow ratio, defined as the amount of reactant discharge to channel to the amount consumed by the electrochemical reaction. That is:

$$\xi_a = x_{H2,in} U_{a,in} \frac{2F}{I_{ref}} \frac{A_{a,in}}{A} \tag{1}$$

$$\xi_c = x_{O2,in} U_{C,in} \frac{4F}{I_{ref}} \frac{A_{C,in}}{A} \tag{2}$$

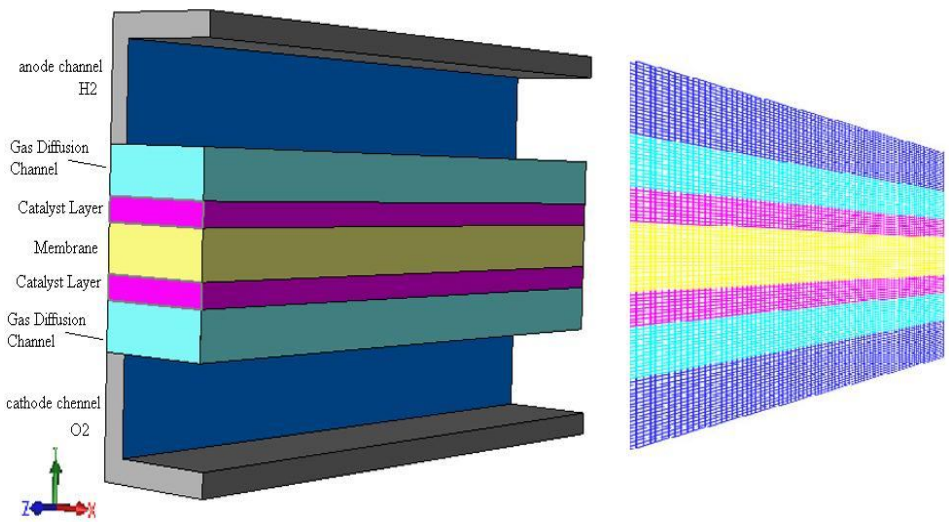

Fig.1: schematic of fuel cell layers and 2-D computational domain

The governing equations used in the present, two-phase model are given in this section. A unified form of the governing equations is used to model the component of fuel cell.

Continuity and Momentum equation for the two-phase mixture in open channel and the porous GDL are presented as follows:

$$\nabla.(\rho\varepsilon u) = 0 \tag{3}$$

Flow channel is considered non-porous therefore ε quantity is one for this region and for CL and GDL it is number between 0 and 1. The total mixture density (including both phases) is:

$$\rho = (1-s)\rho_g + s\rho_l \tag{4}$$

$$\frac{\partial(\rho uu)}{\partial x} + \frac{\partial(\rho uv)}{\partial y} = -\frac{\partial P}{\partial x} + \frac{\partial}{\partial x}\left(\mu\frac{\partial u}{\partial x}\right) + \frac{\partial}{\partial y}\left(\mu\frac{\partial u}{\partial y}\right) - \varepsilon\frac{\mu}{K}u \tag{5}$$

$$\frac{\partial(\rho vu)}{\partial x} + \frac{\partial(\rho vv)}{\partial y} = -\frac{\partial P}{\partial y} + \frac{\partial}{\partial x}\left(\mu\frac{\partial v}{\partial x}\right) + \frac{\partial}{\partial y}\left(\mu\frac{\partial v}{\partial y}\right) - \varepsilon\frac{\mu}{K}v \tag{6}$$

The two-phase mixture viscosity is obtained from:

$$\mu = \frac{\rho_l s + \rho_g(1-s)}{\frac{k_{rg}}{\nu_g} + \frac{k_{rl}}{\nu_l}} \tag{7}$$

Here, the liquid water saturation,s, is defined as the volume fraction of open pores occupied by liquid water, which is a key parameter characterizing the two-phase flow.

$$s = \frac{V_L}{V_{pore}} \tag{8}$$

Where the physical properties of the two-phase mixture are defined as:

$$\varepsilon\rho_l u_l = j_l + \varepsilon\lambda_l\rho u \tag{9}$$

$$\varepsilon\rho_g u V_g = j_g + \varepsilon\lambda_g\rho u \tag{10}$$

j_l represent the phase diffusion between the liquid and the mixture momentum. Similarly j_g is the phase diffusion between the gas phase and the mixture momentum,

$$j_g = -j_l \tag{11}$$

$$j_l = \frac{\lambda_l\lambda_g K}{\nu}[\nabla P_C] \tag{12}$$

Where ν is the mixture kinematic viscosity and λ is the relative mobility, with the value for liquid and gas phases obtained from]:

$$\lambda_l = \frac{\frac{k_{rl}}{\nu_l}}{\frac{k_{rg}}{\nu_g} + \frac{k_{rl}}{\nu_l}} \quad (13)$$

$$\lambda_g = 1 - \lambda_l \quad (14)$$

The relative permeability for the phases is obtained from the experimental equations as Follows:

$$k_{rg} = (1 - s)^3 \quad (15)$$

$$k_{rl} = s^3 \quad (16)$$

The capillary pressure can be further expressed as:

$$P_C = P_l - P_g = \sigma \cos(\theta_C) \left(\frac{\varepsilon}{K}\right)^{\frac{1}{2}} J(s) \quad (17)$$

σ Is the surface tension of water and θ_C is the contact angle of water on the porous material. *J*(s) is the Leverett function, which takes the following form:

$$J(s) = \begin{cases} 1.417(1 - s) - 2.120(1 - s)^2 + 1.263(1 - s)^3 & \text{for } \theta_C < 90^0 \\ 1.417s - 2.120s^2 + 1.263s^3 & \text{for } \theta_C > 90^0 \end{cases} \quad (18)$$

P^{sat} , is obtained at the mixture temperature:

$$\log_{10} P^{sat} = -2.1794 + 0.02953(T - 273.15) - 9.1837 \times 10^{-5}(T - 273.15)^2 \times 10^{-7}(T - 273.15)^3 \quad (19)$$

To predict the content of liquid water an equation for the saturation levels,s is required. The value of s can be somehow predicted using an algebraic equation [10]. However, at the cost of complexity and more computation time a separate PDE for the conservation of liquid water can been derived and solved to determine the saturation levels s. This guarantees the conservation of the water (liquid water +water vapor) by adding the conservation equations of the liquid water (Eq. (20)) and the water vapor (Eq. (21)). The continuity equation of the liquid water is:

$$\nabla.\left(\varepsilon s \rho_l u_l\right) = \varepsilon q_l \quad (20)$$

$$\nabla.\left(\varepsilon s \rho_g u_g\right) = -\varepsilon q_l \quad (21)$$

q_l Is a simplified switch function between condensation and /or evaporation of liquid water under these non-equilibrium conditions .When the partial pressure of water vapor

Exceeds the saturation pressure of water, liquid water may form and occupy the pores in the porous medium. Conversely, the liquid water will evaporate if the partial pressure of water vapor is less than the saturation pressure of water:

$$q_l = \begin{cases} k_{cond}\varepsilon(1 - s)\frac{M^{H2O}.P_g}{RT}\left(x_g^{H2O} - x_{sat}^{H2O}\right) & \text{if } x_g^{H2O} \geq x_{sat}^{H2O} \\ k_{vap}\varepsilon s \rho_l P_g\left(x_g^{H2O} - x_{sat}^{H2o}\right) & \text{if } x_g^{H2O} \leq x_{sat}^{H2O} \end{cases} \quad (22)$$

Where k_c and k_e are the vapor condensation and evaporation rate constants, x^{H2O} is the mole fraction of water vapor.

The species equation for the gaseous species is as follows:

$$\nabla.(\rho\varepsilon u Y_i) - \nabla.\left(\rho\varepsilon D^{eff}\nabla Y_i\right) = S_k \qquad k = H_2O, H_2, O_2 \quad (23)$$

$$D^{eff} = D \times \varepsilon^{1.5} \quad (24)$$

Charge conservation:

In a fuel cell, the potential gradient effect causes electrons and protons to move along individual paths. Solid phases control the movement of electrons. Electron transport generally occurs only in the bipolar plates, the diffusion layers, and the catalyst layers. However, ionomer phases control the motion of protons, which occurs in the catalyst layer and the electrolyte membrane. Potential fields in these two media are described as follows:

In the solid phase:

$$\nabla.(\Gamma_s \nabla V_s) = S \quad (25)$$

$$\nabla.(\Gamma_s \nabla V_s) = S \quad (26)$$

Total electrochemical potential lose consist of three terms as follows:

$$\eta_{a,tot} = \eta_{a,act} + \eta_{a,elec} + \eta_{a,pro} \quad (27)$$

$$\eta_{a,elec} = \left|V_s - V_{s,ref}\right| \quad (28)$$

$$\eta_{a,pro} = \left|V_m - V_{m,ref}\right| \quad (29)$$

$$\eta_{c,tot} = \eta_{c,act} + \eta_{c,elec} + \eta_{c,pro} \quad (30)$$

$$\eta_{c,elec} = |V_s - V_{s,ref}| \quad (31)$$

$$\eta_{c,pro} = |V_m - V_{m,ref}| \quad (32)$$

S index indicate solid phase that consist of cathode and anode side GDL,CL .

For membrane potential equation is:

$$\nabla.(\Gamma_m \nabla V_m) = S \quad (33)$$

$$\eta_{m,pro} = V_{m,c} - V_{m,a} \quad (34)$$

$$V_{cell} = E_{rev} - \eta_{a,tot} - \eta_{c,tot} - \eta_{m,pro} \quad (35)$$

$$E_{rev} = 1.23 - 0.9 \times 10^{-5}(T - 298) \quad (36)$$

Where Γ_m , Γ_s and S denote electron conductivity, proton conductivity and consumption rates of charge and product in the electrochemical reaction in the catalyst layer, respectively. In these expressions, S is equal to j_a and j_c that are the transfer current densities at the anode and cathode, respectively, which can be calculated based the Bulter-Volumer equations follows:

$$j = a^{eff} j_{0,a}^{ref} \left(\frac{C_{H2}}{C_{H2,ref}}\right)^{\frac{1}{2}} \left(\frac{\alpha_a + \alpha_c}{RT}.F.\eta\right) \quad \text{in anode} \quad (37)$$

$$j = a^{eff} j_{0,c}^{ref} \left(\frac{C_{O2}}{C_{O2,ref}}\right) \exp\left(-\frac{\alpha_c}{RT}.F.\eta\right) \quad \text{in cathode} \quad (38)$$

The continuity criterion of current leads to:

$$I_{AVE} = \sum_{j=1}^{N_c} j_{C,j} \times Vol_j = \sum_{j=1}^{N_a} j_{a,j} \times Vol_j \quad (39)$$

Vol_j Is a node volume in computational domain.

Energy conservation:

$$\nabla.(\rho\varepsilon u c_p T) - \nabla.(k^{eff}\varepsilon\nabla T) = \varepsilon S_T \quad (40)$$

S_T Is a source term due to heat generation inside the cell.

Table.1 shows the source term related to governing equations in various regions of PEMFC.

Table.1 Source terms for governing equations in various regions of a PEMFC

	Gas channel	Diffusion layer	Catalyst layer	Membrane
Species O_2	$S_o = 0$	$S_o = 0$	$S_O = -\left(\frac{i_c}{4F}\right) M_O$	$S_o = 0$
H_2	$S_h = 0$	$S_h = 0$	$S_h = -\left(\frac{i_a}{2F}\right) M_h$	$S_h = 0$
Charge				
Solid phase	$S_{\phi,s} = 0$	$S_{\phi,s} = 0$	$S_{\phi,s} = -j$	$S_{\phi,s} = 0$
Membrane phase	$S_{\phi,m} = 0$	$S_{\phi,m} = 0$	$S_{\phi,m} = j$	$S_{\phi,m} = 0$
Energy	$S_T = 0$	$S_T = 0$	$S_T = i\left(\eta + T\frac{dV_{oc}}{dT}\right) + \frac{I^2}{k_m}$	$S_T = \frac{I^2}{k_m}$

3. SOLUTION PROCEDURE

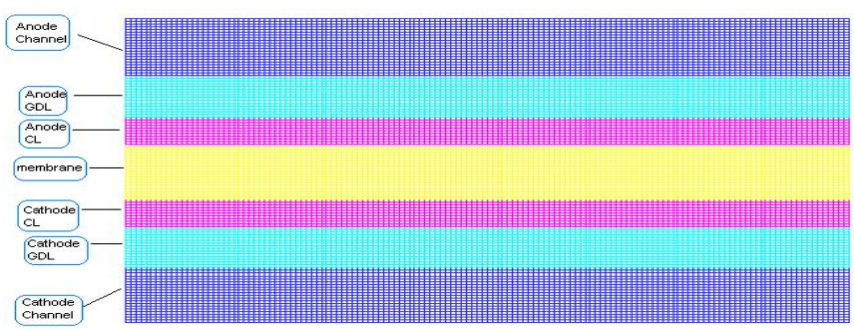

Fig.2: 2-D computational domain

A unified single domain approach with a single set of governing equations is applied to all regions. The computational Domain is divided into a number of sub-domains and different sets of conservation equations are developed

for different sub-domains and the interfacial boundary conditions establish the connection between these equations. Therefore this model has a set of coupled non-linear partial differential equations including conservations of mass, momentum, species, energy and charge with electrochemical relations. The grid network used for numerical modeling is shown in Fig.2 with geometrical parameters listed in Table 2.

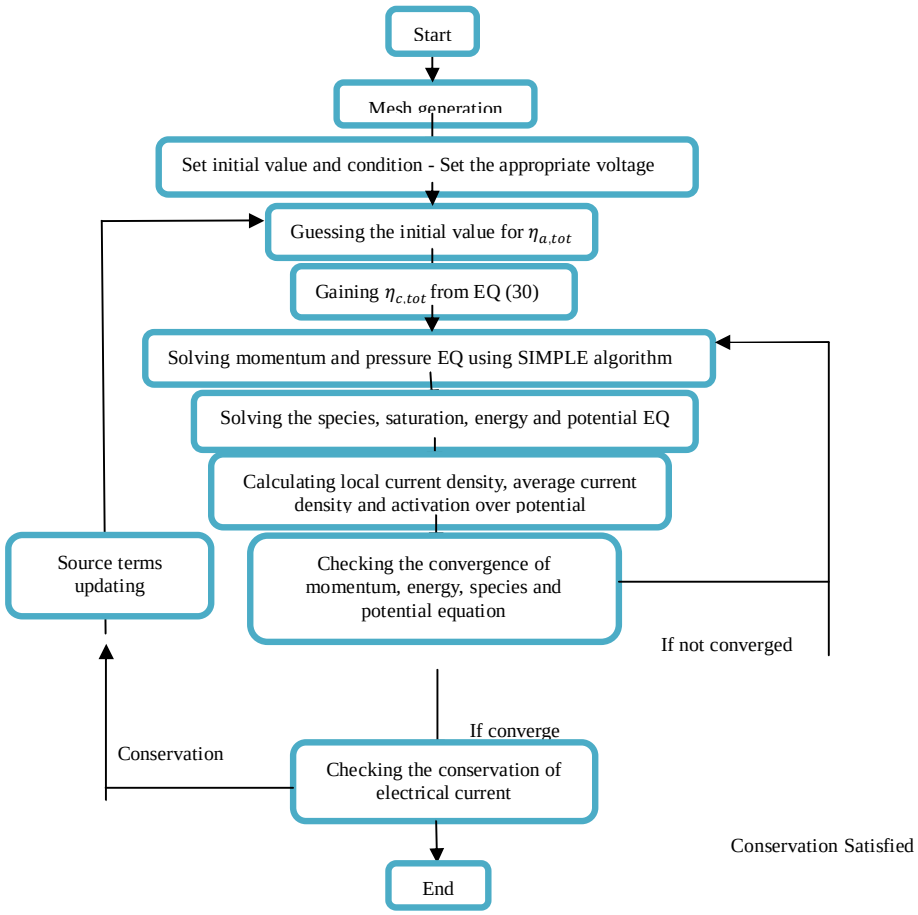

Fig.3 Flowchart for solving the equation

Table. 2 properties and geometrical parameters

Table.2	**Model parameters for basic case**	
Parameter	Symbol	Value
Gas channel length	L	70 mm
Gas channel thickness	H_{ch}	1 mm
Diffusion layer thickness	H_d	0.3 mm
Catalyst layer thickness	H_{cl}	0.01 mm
Membrane thickness	H_m	0.058 mm
Gas channel inlet temperature	T_{in}	353 K
Anode/cathode pressure	p_a/p_c	$1/1atm$
Fuel/air stoichiometric flow ratio	ξ_a/ξ_c	3/3
Anode exchange current density multiply specific area	$aj_{a,ref}$	$5.0 \times 10^7\ A\ m^{-3}$
Cathode exchange current density multiply specific area	$aj_{C,ref}$	$120\ A\ m^{-3}$
Anode transfer coefficient	α_a	.5
Cathode transfer coefficient	α_c	.5
Porosity of diffusion layer	ε_d	.3
Porosity of catalyst layer	ε_{cl}	.28
Absolute permeability	K	$1.76 \times 10^{-11}\ m^2$
Solid phase conductivity	Γ_s	$53\ S\ m^{-1}$
Membrane phase conductivity	Γ_m	$6\ S\ m^{-1}$
Surface tension	σ	$0.0625\ N\ m^{-1}$
Current collector thermal conductivity	k_c	$150\ W\ m^{-1}\ K^{-1}$
Diffusion layer thermal conductivity	k_d	$150\ W\ m^{-1}\ K^{-1}$

The set of equations explained in Section 2 are discretized using the power law method. A code was developed for solution of the set of PDE's using the SIMPL scheme of Patankar [17]. Stringent numerical tests were carried out to ensure that the Solution was independent of grid size. The coupled set of equations was solved iteratively, and the solution was checked to be convergent when the relative error in each field between two consecutive iterations was less than 10^{-5}. The flowchart for this simulation is shown in Fig. 3.

4. RESULT AND DISCUSSION

Fig. 4 presents the comparison between the numerical and experimental polarization curves as verification. As shown in this figure, reasonable agreement between the present study and the experimental data [18] can be seen. difference between two curve result of some simplification as considering the two dimensional model instead of three dimensional model. Comparison between isothermal and non isothermal polarization curve shows that non isothermal model is much similar to experimental curve than isothermal one.

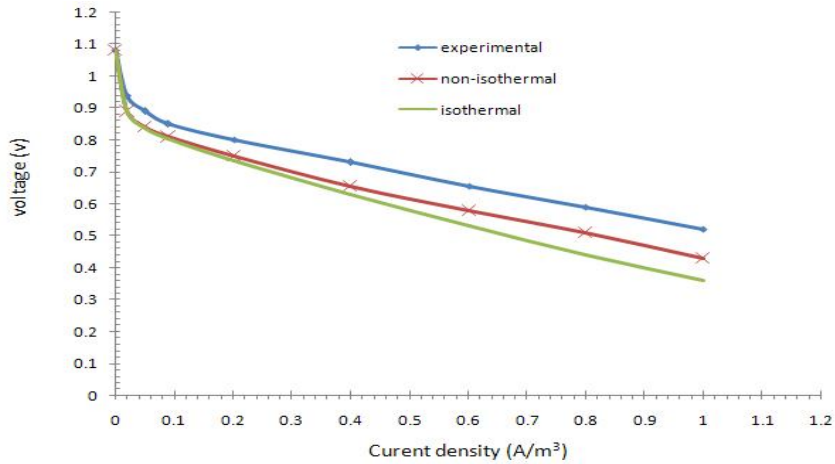

Fig.4 polarization curve

The temperature distribution on the surface of the fuel cell is shown in Fig. 5. The temperature tends to become higher at the flow entrance and near the middle region. It is thought that this high temperature at entrance region is caused by high concentration of hydrogen and oxygen supplied at the flow inlet. The maximum temperature difference is observed to be 4.5 c^o near the inlet and at the interface between membrane and catalyst layer in the cathode side. Unlike channels, velocity in the membrane–electrode assembly is very low; therefore heat generation in the cell is carried downstream smaller and is removed primarily through the gas diffusion layer by conduction.

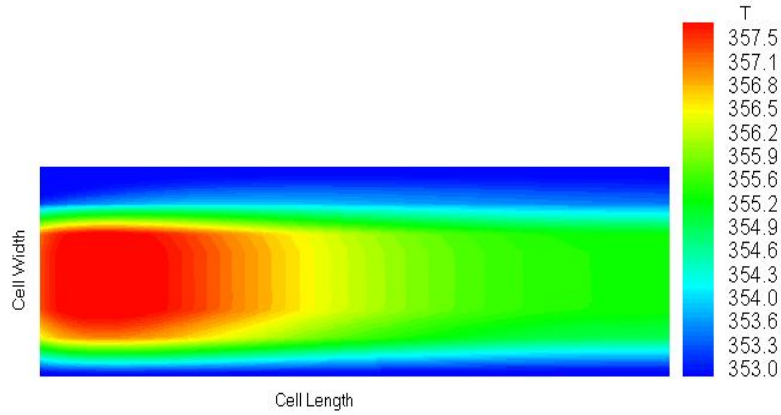

Fig. 5 The temperature distribution on the surface of the fuel cell

The numerically predicted liquid saturation distribution at cathode side GDL-CL interface

Is shown in Fig. 6 (where the water production takes place) for both the isothermal and non-isothermal models. The water may condense, but this does not occur until the water vapor concentration in the gas reaches the saturation level. The condensation with its location directly related to the local temperature and condensation front is then pushed

downstream. In the non-isothermal model, up to a certain point along its lengths, the GDL is free of any liquid water after which the stream of liquid water starts to appear. In the isothermal model, the water condensation and accumulation occur further upstream towards the inlet of the channel, where the amount of liquid saturation is higher in the isothermal compared with the non-isothermal model. This is because in non-isothermal model, the temperature is higher than that of the isothermal model. The increase in temperature causes an increase in saturation pressure, so less water vapor changes phase.

The liquid saturation level for isothermal and non-isothermal models at cathode GDL/catalyst layer interface is shown in Fig. 6. In both cases, the minimum liquid saturation occurs near the inlet and increases in the flow direction due to increasing water production in the channel length. The amount of liquid saturation along the channel in the isothermal model is more than the Non-isothermal one, where the maximum deviation for both cases appears at the entrance where the cell temperature is highest.. Further along the channel the temperature drop causes the deviation to decrease as well where the vapor saturation concentration is a strong function of temperature.

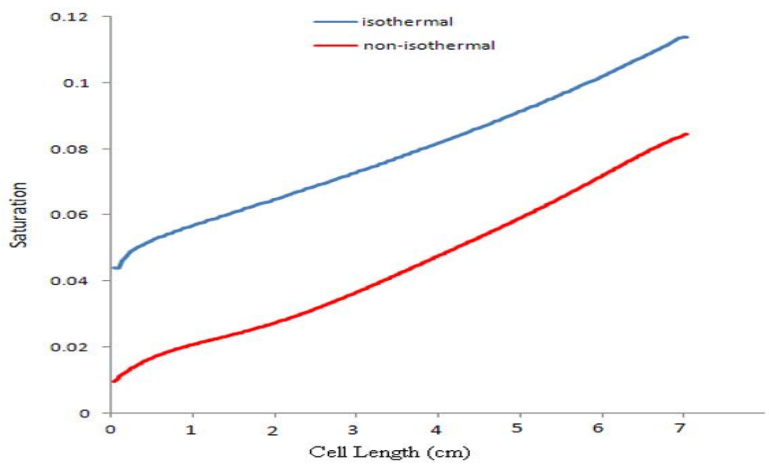

Fig.6: liquid saturation distribution at cathode side GDL-CL interface

Fig. 7 shows the effect of the temperature gradient on I–P power density curves. For operating current density < 0.4□/□^{3}, the power density curves for isothermal and non-isothermal almost coincide, approximately at this current density water molecules are in vapor phase indicating negligible saturation effects [19]. However, at operating current density > 0.4□/□^{3}, the saturation effect is profound. The difference of output power density magnitude between to model increase with increasing the current density, because at non- isothermal model water vapor pressure is a function of temperature and increasing the temperature cause low amount of water vapor condense and therefore porous paths for oxygen diffusion is not clog bye water drops, so voltage lose due to oxygen mass diffusion clogging and oxygen dilution decrease.

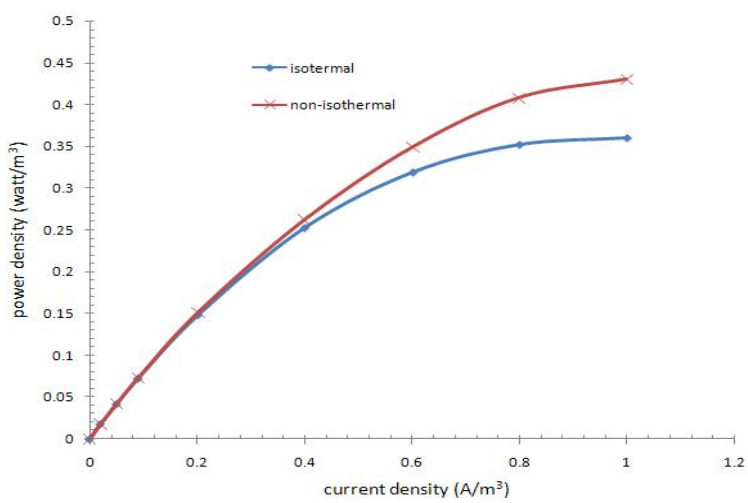

Fig.7: the effect of the temperature gradient on I–P power density

At previous some research work has been done to explore the efficacy of saturation on cell performance [10, 11,16] but variation of saturation level and its location by temperature gradient along the cell was not seen in previous fuel cell literature, therefore need to research in this section was indispensable. This study was done to response the above demand. In future work it is necessary to consider three-dimensional model to come closer approach to real fuel cell's transport phenomena simulation**.**

Nomenclature

Aj_0^{ref}	Exchange current density, A m^{-3}	V_{cell}	Operating voltage, V
D	Mass diffusivity, m^2 s^{-1}	y	Y direction coordinate, m
F	Faraday constant,96,487 C/mol	Greek	
i	Local Current density, A m^{-2}	α_a	Electrical transfer coefficient in forward reaction
I	Average current density in the fuel cell, A m^{-2}	α_C	Electrical transfer coefficient in backward reaction
j	Transfer current density, A m^{-3}	ϵ	Porosity
k_{ccond}	Coefficient of water vapor condensation rate, s^{-1}	η	Over potential, Volt
k_{rl}	Relative permeability of the liquid water	θ	Contact angle of water on the porous material, arc
K	Permeability, m^2	λ	relative mobility
k_{rg}	Relative permeability of the gaseous mixture	μ	Viscosity, kg m^{-1} s^{-1}
M	Molecular weight, kg mol^{-1}	ρ	Density, kg m^{-3}
p	Pressure, atm	Γ_m	Proton conductivity, S m^{-1}
p_c	Capillary pressure, atm	Γ_s	Electron conductivity, Sm^{-1}
R	Universal gas constant, 8.314 mol^{-1} K^{-1}	V_S	Electronic phase potential, V
s	Ratio of the liquid water volume to the pore volume(saturation)	V_m	Ionic phase potential, V
S	Source term in equations	a	Anode
$\vec{u}$	Velocity vector, m s^{-1}	c	Cathode
v	Velocity vector, m s^{-1}	k	kth Species of the mixture
Vol	Volume, m^3	l	Liquid phase

REFERENCES

[1] Matthew M. Mench, 2008.Fuel cell engines, John Wiley & Sons, Inc, PP: 121-122, 9-10,168-170

[2] Lixin You a, Hongtan Liu, 2002. A two-phase flow and transport model for the cathode of PEM fuel cells. International Journal of Heat and Mass Transfer 45 (2002) 2277–2287

[3] Jin Hyun Nam 1, Massoud Kaviany, Effective diffusivity and water-saturation distribution in single-and two-layer PEMFC diffusion medium. International Journal of Heat and Mass Transfer 46 (2003) 4595–4611

[4] Y.Wang, C.Y.Wang, A Non-Isothermal, Two-Phase Model for Polymer Electrolyte Fuel Cells, J. Electrochem Soc, 153 (2006) A1193–1200.

[5] J.J. Hwang, A complete two-phase model of a PEM fuel cell, J. Power Sources 164 (2007) 174–181.

[6] Z.H. Wang, C.Y. Wang, K.S. Chen, Two phase flow and transport in the air cathode of proton exchange membrane fuel cells,J. Power Sources 94 (2001) 40–50.

[7] U. Pasaogullari, C.Y.Wang, Two-phase modeling and flooding prediction of polymer electrolyte fuel cells, J. Electrochem Soc, 152 (2005) A380–A390.

[8] T. Berning, N. Djilali, Three-dimensional computational analysis of transport phenomena in a PEM fuel cell—a parametric study, J. Power Sources 124 (2003) 440–452.

[9] T. Berning, N. Djlali, A 3D, Multiphase, Multi component Model of the Cathode and Anode of a PEM Fuel Cell J. Electrochem Soc, 150 (2003) A1589–A1598.

[10] Y.Wang, C.Y.Wang, Ultra large-scale simulation of polymer electrolyte fuel cells, J. Power Sources 153 (2006) 130–135.

[11] Maher A.R. Sadiq Al-Baghdadi, Haroun A.K. Shahad Al-Janabi, Parametric and optimization study of a PEM fuel cell performance using three-dimensional computational fluid dynamics model, Renewable Energy 32 (2007) 1077–1101

[12] T.berning,D.M .Lu,N.Djlali, Three- Dimensional computational analysis of transport phenomena in a PEM fuel cell, J. Power Sources 106 (2002) 284–294

[13]Ugur Pasaogullari, Chao-Yang Wang, Two-phase transport and the role of micro-porous layer in polymer electrolyte fuel cells, Electrochimica Acta 49 (2004) 4359–4369

[14] Z.H. Wanga, C.Y. Wanga, K.S. Chen, Two-phase flow and transport in the air cathode of proton exchange membrane fuel cells, Journal of Power Sources 94 (2001) 40-50

[15] Y.Wang, C.Y.Wang, A Non-Isothermal, Two-Phase Model for Polymer Electrolyte Fuel Cells, J. Electrochem Soc. 153 (2006) A1193–1200.

[16] H. Ju, C.Y. Wang, S. Cleghorn, U. Beuscherb, Nonisothermal Modeling of Polymer Electrolyte Fuel Cells II. Parametric Study of Low-Humidity Operation, Journal of the Electrochemical Society, 153 (2) A249-A254 (2006)

[17] S.V. Patankar, Numerical Heat Transfer and Fluid Flow, Hemisphere, PA, New York, 1980.

[18] E.A. Ticianelli, C.R. Derouin, A. Redondo, S. Srinivasan, Methods to Advance Technology of Proton Exchange Membrane Fuel Cells J. Electrochem. Soc. 135(1988) 2209-2214

[19] Lixin You a, Hongtan Liu,A two-phase flow and transport model for the cathode of PEM fuel cells International Journal of Heat and Mass Transfer 45 (2002) 2277–2287